

Numerical conformal mappings onto the linear slit domain

Kaname Amano · Dai Okano · Hidenori Ogata ·
Masaaki Sugihara

Received: 19 May 2011 / Revised: 23 October 2011 / Published online: 17 April 2012
© The Author(s) 2012. This article is published with open access at Springerlink.com

Abstract We propose a numerical method for the conformal mapping of unbounded multiply connected domains exterior to closed Jordan curves C_1, \dots, C_n onto a canonical linear slit domain, which is the entire plane with linear slits S_1, \dots, S_n of angles $\theta_1, \dots, \theta_n$ arbitrarily assigned to the real axis, respectively. If $\theta_1 = \dots = \theta_n = \theta$ then it is the well-known parallel slit domain, which is important in the problem of potential flows past obstacles. In the method, we reduce the mapping problem to a boundary value problem for an analytic function, and approximate it by a linear combination of complex logarithmic functions based on the charge simulation method. Numerical examples show the effectiveness of our method.

Keywords Conformal mapping · Multiply connected domain · Potential flow · Charge simulation · Fundamental solution

Mathematics Subject Classification 30C30 · 65E05

This work was supported by Grant-in-Aid for Scientific Research (B) 19340024, Japan Society for the Promotion of Science.

K. Amano (✉) · D. Okano
Department of Electrical and Electronic Engineering and Computer Science,
Graduate School of Science and Engineering, Ehime University,
3 Bunkyo-cho, Matsuyama 790-8577, Japan
e-mail: amano@cs.ehime-u.ac.jp

H. Ogata
Department of Communication Engineering and Informatics, Graduate School of Informatics
and Engineering, The University of Electro-Communications, 1-5-1 Chofu-ga-Oka,
Chofu 182-8585, Japan

M. Sugihara
Department of Mathematical Informatics, Graduate School of Information Science and Technology,
The University of Tokyo, 7-3-1 Hongo, Bunkyo-ku, Tokyo 113-8656, Japan

1 Introduction

Conformal mappings are familiar in science and engineering. However, exact mapping functions are not known except for some special domains, and the numerical conformal mapping has been an attractive subject in scientific computation [13, 16, 21, 29, 48].

Symm [45–47] proposed the well-known integral equation method for the conformal mapping of a simply connected domain bounded by a closed Jordan curve onto the unit disk, of its exterior onto the exterior of the unit disk, and of a doubly connected domain onto a concentric circular annulus. In the method, he expressed an unknown harmonic function by a single-layer logarithmic potential and derived a linear Fredholm integral equation of the first kind; and numerically approximated its source density by a step function. Gaier [17, 18] proved the existence and uniqueness of the solution. Hayes et al. [20] approximated the source density by piecewise quadratic polynomials, and improved the accuracy of numerical results. Hough and Papamichael [22, 23] approximated the source density by spline functions blended with suitable singular functions, and overcame difficulties associated with corner singularities. On the other hand, Amano [1, 2] applied the charge simulation method (the fundamental solution method), which was known as a fast, accurate solver for the Dirichlet problem of Laplace's equation, to the same problems as Symm studied. In the method, he approximated a pair of harmonic functions by a linear combination of complex logarithmic functions, and obtained a simple form of approximate mapping functions with high accuracy for problem domains with no reentrant corners. Numerically, we have only to solve a system of linear equations without integration. In the case of conformal mapping from standard domain onto problem domain, nonlinear integral equations are solved by the fast Fourier transform and various iterative methods [14, 15, 19].

Recently, conformal mappings of multiply connected domains have been studied actively. It is known that two domains can be conformally mapped onto each other if, and only if, they agree in connectivity n , and $3(n - 2)$ ($n \geq 3$) conformal invariants called moduli. Hence, canonical domains that specify geometric characters without fixing moduli are introduced. They often have slits, and the following five domains listed in Nehari [34] are well known: the parallel slit domain, the circular slit domain, the radial slit domain, the circle with concentric circular slits, and the circular ring with concentric circular slits. Koebe [28] formerly gave thirty-nine canonical slit domains, which contained domains with a mixture of circular and radial slits called the circular and radial slit domain. The circular domain, all of whose boundary curves are circles, is another important canonical domain without slits. DeLillo et al. [7, 10] extended Fornberg's method [14, 15] to the case of multiply connected domains, and gave a method for numerical conformal mapping from an unbounded circular domain onto an unbounded multiply connected domain. DeLillo et al. [11] also generalized the Schwarz–Christoffel mapping to multiply connected domains, and derived a formula for conformal mapping from an unbounded circular domain onto an unbounded polygonal domain. Crowdny and Marshall [9] constructed analytical formulae for conformal mapping from a bounded circular domain onto the five canonical slit domains above mentioned, and DeLillo et al. [12] from an unbounded circular domain onto the circular and radial slit domain. Crowdny [8] constructed also an analytical solution for uniform potential flows past multiple cylinders. The charge simulation method is applicable

also to the problem of conformal mappings of multiply connected domains. We proposed a method for the conformal mapping of unbounded multiply connected domains onto the parallel slit domain, the circular slit domain and the radial slit domain [3, 4], and onto the circular and radial slit domain [6]; and for the conformal mapping of bounded multiply connected domains onto the circle and the circular ring with concentric circular slits [41]. The charge simulation method is particularly suited for the conformal mapping from circular domains onto the canonical slit domains.

In this paper, we propose a method for the conformal mapping of unbounded multiply connected domains exterior to closed Jordan curves C_1, \dots, C_n onto a canonical linear slit domain, which is the entire plane with linear slits S_1, \dots, S_n of angles $\theta_1, \dots, \theta_n$ arbitrarily assigned to the real axis, respectively [43]. It is a natural generalization of the parallel slit domain, including the following domains listed in Koebe [28]: the horizontal slit domain ($\theta_1 = \dots = \theta_n = 0$), the horizontal and perpendicular slit domain ($\theta_l = 0$ or $\pi/2$, $l = 1, \dots, n$), the parallel slit domain ($\theta_1 = \dots = \theta_n = \theta$), and the orthogonal slit domain ($\theta_l = \theta$ or $\theta + \pi/2$, $l = 1, \dots, n$).

It seems that the formulation used in the previous approaches by the charge simulation method [2–4, 6, 41], in short Eq. (7), is applicable also to the conformal mapping onto the linear slit domain above described. However, it may lead in this case to a singular coefficient matrix of the linear equations to be solved under some conditions [5]. Therefore, we adopt another formulation suited for this canonical slit domain to resolve the singularity problem, in short Eq. (12) that plays a key role in this paper, and derive a scheme of the numerical conformal mapping. Numerical experiments show the effectiveness of the new formulation. The charge simulation method, when used fittingly, will be a very practical method for approximating the analytic function by a linear combination of complex logarithmic functions as well as the harmonic function by real logarithmic functions.

The contents are as follows. In Sect. 2, we outline the charge simulation method in advance, quoting Eq. (7) as the basic idea of the previous approaches to the numerical conformal mapping. In Sect. 3, we formulate the problem for the conformal mapping of unbounded multiply connected domains onto the linear slit domain. In Sect. 4, we apply the charge simulation method to the problem using Eq. (12), and construct a simple form of approximate mapping function. In Sect. 5, we give supplementary comments on the numerical method using Eq. (7). In Sect. 6, we show numerical examples with some applications to potential flows. In Sect. 7, we make concluding remarks.

2 Charge simulation method

The charge simulation method is originally a potential solver, and has been used in the field of electrical engineering [32, 44]. Katsurada and Okamoto [25, 26] obtained extensive results concerning error bounds and convergence of the method. Kitagawa [27] analyzed the numerical stability of the method. Murota [33] improved the method to be invariant with respect to trivial affine transformations. Ogata et al. [36] proved solvability of the linear equations appearing in the invariant scheme. We here outline the principle of the charge simulation method.

Let D be a domain bounded by a closed Jordan curve C in the $z = x + iy$ plane, and consider the Dirichlet problem of two-dimensional Laplace's equation

$$\Delta g(z) = 0 \quad \text{in } D, \quad g(z) = b(z) \quad \text{on } C, \quad (1)$$

where $b(z)$ is the boundary data. We identify the real (x, y) plane with the complex z plane, and abbreviate $g(x, y), b(x, y)$ as $g(z), h(z)$.

The charge simulation method approximates the solution by

$$g(z) \simeq G(z) = \sum_{j=1}^N Q_j \log |z - \zeta_j|, \quad (2)$$

i.e., a linear combination of logarithmic functions (fundamental solutions of the Laplace equation). The singular points $\zeta_1, \dots, \zeta_N \notin \overline{D}(= D \cup C)$ called *the charge points* are placed outside the problem domain, and (2) exactly satisfies Laplace's equation. The unknown real constants Q_1, \dots, Q_N called *the charges* are determined to satisfy the boundary condition at the collocation points $z_1, \dots, z_N \in C$ placed on the boundary,

$$\sum_{j=1}^N Q_j \log |z_k - \zeta_j| = b(z_k), \quad k = 1, \dots, N, \quad (3)$$

which is called *the collocation condition*. That is to say, they are the solution of a system of linear equations (3). Once Q_1, \dots, Q_N are determined, $g(z)$ is approximated by $G(z)$ at any point in D . If D is bounded, from the maximum principle for harmonic functions, $G(z)$ takes its maximum error somewhere on the boundary,

$$|G(z) - g(z)| \leq \max_{z \in C} |G(z) - b(z)|. \quad (4)$$

It is known that the error decays exponentially with respect to N under some condition [25, 26], which results in high accuracy.

In the numerical conformal mapping [1–4, 6, 41], we reduced the problem of finding the mapping function $f(z)$ to the problem of finding a harmonic function $g(z)$ and its harmonic conjugate $h(z)$ so that $g(z)$ was subject to a Dirichlet type of boundary condition. If $g(z)$ is approximated by (2), then $h(z)$ by

$$h(z) \simeq H(z) = \sum_{j=1}^N Q_j \arg(z - \zeta_j) \quad (5)$$

up to a constant. As a result, we have an approximation of the pair of harmonic functions in the form of linear combination of complex logarithmic functions,

$$\begin{aligned} g(z) + i h(z) &\simeq G(z) + i H(z) \\ &= Q_0 + \sum_{j=1}^N Q_j (\log |z - \zeta_j| + i \arg(z - \zeta_j)) \\ &= Q_0 + \sum_{j=1}^N Q_j \log(z - \zeta_j), \end{aligned} \quad (6)$$

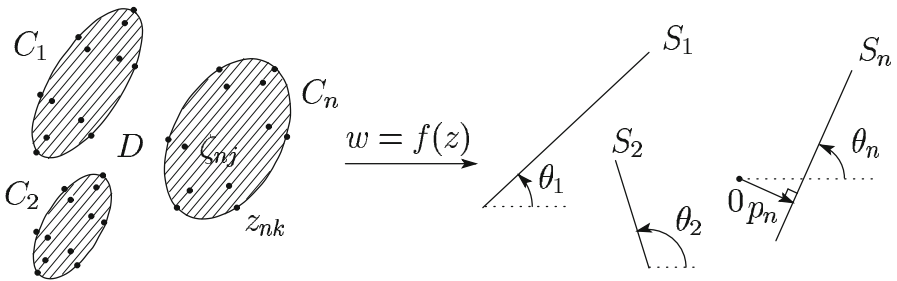


Fig. 1 Conformal mapping onto the linear slit domain, together with charge points and collocation points used in the charge simulation method

where Q_0 is a complex constant; and determine the unknown constants Q_0, Q_1, \dots, Q_N so as to approximately satisfy the requirements for $f(z)$.

This approach [1,2] was effective also in the case of various shapes of multiply connected canonical slit domains [2–4,6,41] in principle by rewriting (6) into

$$\begin{aligned} g(z) + i h(z) &\simeq G(z) + i H(z) \\ &= Q_0 + \sum_{l=1}^n \sum_{j=1}^{N_l} Q_{lj} (\log |z - \xi_{lj}| + i \arg(z - \xi_{lj})) \\ &= Q_0 + \sum_{l=1}^n \sum_{j=1}^{N_l} Q_{lj} \log(z - \xi_{lj}), \end{aligned} \quad (7)$$

where Q_{lj} and ξ_{lj} are for boundary curves C_l , $l = 1, \dots, n$ of the problem domain (see Fig. 1). However, in the case of linear slit domain considered in Sect. 3, some technical ingenuity is needed as described in Sect. 4. Because, Eq. (7) may lead to a singular coefficient matrix of the linear equations to be solved under some conditions as described in Sect. 5.

3 Mapping theorem and the problem

Let D be an unbounded domain exterior to closed Jordan curves C_1, \dots, C_n in the $z = x + iy$ plane. Consider the conformal mapping of D onto the linear slit domain, which is the entire $w = u + iv$ plane with linear slits S_1, \dots, S_n of angles $\theta_1, \dots, \theta_n$ to the real axis as shown in Fig. 1. We suppose that both planes include the point at infinity. We start from the following theorem.

Theorem 1 *For the angles $\theta_1, \dots, \theta_n$ arbitrarily assigned, there exists a unique analytic function $w = f(z)$ such that (i) conformatly maps D onto the linear slit domain, (ii) satisfies $f(\infty) = \infty$, and (iii) has the Laurent expansion near $z = \infty$ of the form*

$$f(z) = z + \frac{a_1}{z} + \frac{a_2}{z^2} + \dots . \quad (8)$$

If $\theta_1 = \dots = \theta_n = \theta$ then the linear slit domain is the parallel slit domain [34]. Shiba [43] proved Theorem 1 in a more general context as an extension of the mapping onto the parallel slit domain. We aim to construct an approximate function of $f(z)$, and all the coefficients of the Laurent expansion (8) as well.

We express the mapping function as

$$f(z) = z + a(z), \quad (9)$$

where $a(z)$ is an analytic function in D . It should be noted that $a(z)$ is not written as $g(z) + ih(z)$ for the reason described at the beginning of the next section.

The function $a(z)$ should satisfy the following conditions.

1. Normalization condition: From (8),

$$\lim_{z \rightarrow \infty} (f(z) - z) = 0, \quad \text{i.e.,} \quad a(\infty) = 0. \quad (10)$$

2. Boundary condition: $f(z)$ maps C_1, \dots, C_n onto S_1, \dots, S_n of the angles $\theta_1, \dots, \theta_n$, so that

$$\begin{aligned} \operatorname{Im}(e^{-i\theta_m} f(z)) &= p_m, \quad \text{i.e.,} \quad \operatorname{Im}(e^{-i\theta_m} a(z)) - p_m = -\operatorname{Im}(e^{-i\theta_m} z), \\ z \in C_m, \quad m &= 1, \dots, n, \end{aligned} \quad (11)$$

where p_m is the unknown signed distance from the origin $w = 0$ to the linear line containing S_m .

From the existence and uniqueness of the mapping function, the problem is now to find $a(z)$ satisfying (10), (11) together with p_1, \dots, p_n . It should be noted again that (11) is a condition for $a(z)$, not for $g(z)$, unlike the preceding problems [1–4, 6, 41].

4 Numerical method

We apply the charge simulation method to the unknown function as

$$a(z) \simeq A(z) = Q_0 + i \sum_{l=1}^n e^{i\theta_l} \sum_{j=1}^{N_l} Q_{lj} \log(z - \zeta_{lj}), \quad (12)$$

where the charge points ζ_{lj} are placed inside C_l , i.e., outside \overline{D} . Equation (12) is slightly different from (7) used in the previous approaches [2–6, 41], and plays a key role in this paper. It is the reason why we do not write (9) as $f(z) = z + g(z) + ih(z)$ that (12) can not be written as $A(z) = Q_0 + G(z) + iH(z)$ any more so that $G(z)$ is a linear combination of $\log|\cdot|$ functions and $H(z)$ of $\arg(\cdot)$ functions.

We impose the following requirements on the approximate function.

1. Single-valuedness condition: $A(z)$ is single-valued if and only if

$$\int_{C_l} dA(z) = i \int_{C_l} d \sum_{m=1}^n e^{i\theta_m} \sum_{j=1}^{N_m} Q_{mj} \log(z - \zeta_{mj}) = -2\pi e^{i\theta_l} \sum_{j=1}^{N_l} Q_{lj} = 0,$$

i.e.,

$$\sum_{j=1}^{N_l} Q_{lj} = 0, \quad l = 1, \dots, n. \quad (13)$$

2. Normalization condition: From (10), we require

$$A(\infty) = Q_0 + \lim_{z \rightarrow \infty} i \sum_{l=1}^n e^{i\theta_l} \sum_{j=1}^{N_l} Q_{lj} \log(z - \zeta_{lj}) = 0,$$

so that $Q_0 = 0$ under (13), and

$$A(z) = i \sum_{l=1}^n e^{i\theta_l} \sum_{j=1}^{N_l} Q_{lj} \log(z - \zeta_{lj}). \quad (14)$$

3. Collocation condition: We require (14) to satisfy the boundary condition (11) collocationally,

$$\operatorname{Im}(e^{-i\theta_m} A(z_{mk})) - P_m = -\operatorname{Im}(e^{-i\theta_m} z_{mk}),$$

i.e.,

$$\begin{aligned} \sum_{l=1}^n \sum_{j=1}^{N_l} Q_{lj} [\cos(\theta_l - \theta_m) \log |z_{mk} - \zeta_{lj}| - \sin(\theta_l - \theta_m) \arg(z_{mk} - \zeta_{lj})] - P_m \\ = -\operatorname{Im}(e^{-i\theta_m} z_{mk}), \end{aligned} \quad (15)$$

$$z_{mk} \in C_m, \quad k = 1, \dots, N_m, \quad m = 1, \dots, n,$$

where z_{mk} are collocation points and P_m are approximations to p_m .

Equations (13) and (15) make up a set of linear equations for the unknown constants Q_{lj}, P_m . Once they are determined, we obtain $A(z)$ by (14), and an approximate mapping function $F(z) \simeq f(z)$ by substituting it for $a(z)$ in (9).

We use in computation the principal value of the logarithmic function, i.e., the branch of $\log z$ such that $-\pi < \arg z \leq \pi$. Consequently, $\log(z - \zeta_{lj})$ in (14) has the discontinuity of $2\pi i$ on the half line $\{\zeta_{lj} - t \mid t > 0\}$, which causes discontinuities of $A(z)$ in D . Therefore, we change the expression (14) into a form that is mathematically equivalent to (14) and is continuous in D when the principal value is used. We call an approximate mapping function using such an expression of $A(z)$ a *continuous scheme*.

Here we assume that, only for simplicity, C_l is starlike with respect to its inside point ζ_{l0} , and using (13) rewrite (14) into

$$\begin{aligned} A(z) &= i \sum_{l=1}^n e^{i\theta_l} \sum_{j=1}^{N_l} Q_{lj} \log(z - \zeta_{lj}) - i \sum_{l=1}^n e^{i\theta_l} \sum_{j=1}^{N_l} Q_{lj} \log(z - \zeta_{l0}) \\ &= i \sum_{l=1}^n e^{i\theta_l} \sum_{j=1}^{N_l} Q_{lj} \log \frac{z - \zeta_{lj}}{z - \zeta_{l0}}. \end{aligned} \quad (16)$$

The term $\log[(z - \zeta_{lj})/(z - \zeta_{l0})]$ has the discontinuity on the line segment (ζ_{lj}, ζ_{l0}) inside C_l , and (16) is continuous in D when the principal value is used. We have the following:

Scheme 1 When each boundary curve C_l is starlike with respect to its inside point ζ_{l0} , a continuous scheme of the approximate mapping function is given by

$$F(z) = z + A(z), \quad A(z) = i \sum_{l=1}^n e^{i\theta_l} \sum_{j=1}^{N_l} Q_{lj} \log \frac{z - \zeta_{lj}}{z - \zeta_{l0}}, \quad (17)$$

where the unknown constants Q_{lj} , together with P_m , are determined by solving the linear equations

$$\sum_{j=1}^{N_l} Q_{lj} = 0, \quad l = 1, \dots, n, \quad (18)$$

$$\begin{aligned} \sum_{l=1}^n \sum_{j=1}^{N_l} Q_{lj} \left[\cos(\theta_l - \theta_m) \log \left| \frac{\zeta_{mk} - \zeta_{lj}}{\zeta_{mk} - \zeta_{l0}} \right| - \sin(\theta_l - \theta_m) \arg \frac{\zeta_{mk} - \zeta_{lj}}{\zeta_{mk} - \zeta_{l0}} \right] - P_m \\ = -\text{Im}(e^{-i\theta_m} z_{mk}), \\ z_{mk} \in C_m, \quad k = 1, \dots, N_m, \quad m = 1, \dots, n. \end{aligned} \quad (19)$$

Using the approximate mapping function, we have the following:

Remark 1 The coefficients of the Laurent expansion (8) is given by

$$a_k \simeq A_k = -\frac{i}{k} \sum_{l=1}^n e^{i\theta_l} \sum_{j=1}^{N_l} Q_{lj} \zeta_{lj}^k, \quad k = 1, 2, \dots \quad (20)$$

from the Taylor expansion of (17).

If $\theta_1 = \dots = \theta_n = \theta$ then the linear slit domain is the parallel slit domain. In this case, Scheme 1 and Remark 1 are simplified as follows.

Scheme 2 When each boundary curve C_l is starlike with respect to its inside point ζ_{l0} , a continuous scheme of the approximate mapping function is given by

$$F(z) = z + A(z), \quad A(z) = i e^{i\theta} \sum_{l=1}^n \sum_{j=1}^{N_l} Q_{lj} \log \frac{z - \zeta_{lj}}{z - \zeta_{l0}}, \quad (21)$$

where the unknown constants Q_{lj} , together with P_m , are determined by solving the linear equations

$$\sum_{j=1}^{N_l} Q_{lj} = 0, \quad l = 1, \dots, n, \quad (22)$$

$$\begin{aligned} \sum_{l=1}^n \sum_{j=1}^{N_l} Q_{lj} \log \left| \frac{z_{mk} - \zeta_{lj}}{z_{mk} - \zeta_{l0}} \right| - P_m &= -\operatorname{Im}(e^{-i\theta} z_{mk}), \\ z_{mk} &\in C_m, \quad k = 1, \dots, N_m, \quad m = 1, \dots, n. \end{aligned} \quad (23)$$

Remark 2 The coefficients of the Laurent expansion (8) is given by

$$a_k \simeq A_k = -\frac{i e^{i\theta}}{k} \sum_{l=1}^n \sum_{j=1}^{N_l} Q_{lj} \zeta_{lj}^k, \quad k = 1, 2, \dots. \quad (24)$$

Schemes 1 and 2 are, in principle, applicable also to the non-starlike C_l if we redefine the term $\log[(z - \zeta_{lj})/(z - \zeta_{l0})]$ using different points as ζ_{l0} in its concave part. However, in practice, it is not easy to find those points adaptively to the shape of C_l . The following reformulation is usable to resolve the discontinuity problem from the viewpoint of numerical computation. We change the unkowns Q_{lj} to their partial sums

$$Q_l^j = \sum_{k=1}^j Q_{lk}, \quad j = 1, \dots, N_l, \quad l = 1, \dots, n, \quad (25)$$

and using (13), i.e., $Q_l^{N_l} = 0$, rewrite (14) into

$$\begin{aligned} A(z) &= i \sum_{l=1}^n e^{i\theta_l} \sum_{j=1}^{N_l} Q_{lj} \log(z - \zeta_{lj}) \\ &= i \sum_{l=1}^n e^{i\theta_l} \left[Q_l^1 \log(z - \zeta_{l1}) + \sum_{j=2}^{N_l} (Q_l^j - Q_l^{j-1}) \log(z - \zeta_{lj}) \right] \\ &= i \sum_{l=1}^n e^{i\theta_l} \left[\sum_{j=1}^{N_l-1} Q_l^j (\log(z - \zeta_{lj}) - \log(z - \zeta_{lj+1})) + Q_l^{N_l} \log(z - \zeta_{lN_l}) \right] \\ &= i \sum_{l=1}^n e^{i\theta_l} \sum_{j=1}^{N_l-1} Q_l^j \log \frac{z - \zeta_{lj}}{z - \zeta_{lj+1}}. \end{aligned} \quad (26)$$

The term $\log[(z - \zeta_{lj})/(z - \zeta_{lj+1})]$ has the discontinuity on the line segment $(\zeta_{lj}, \zeta_{lj+1})$ inside C_l if charges are so placed that it does not intersect C_l , and (26) is continuous in D when the principal value is used. We have the following:

Scheme 3 Another continuous scheme is given by

$$F(z) = z + A(z), \quad A(z) = i \sum_{l=1}^n e^{i\theta_l} \sum_{j=1}^{N_l-1} Q_l^j \log \frac{z - \zeta_{lj}}{z - \zeta_{lj+1}}, \quad (27)$$

where the unknown constants Q_l^j , together with P_m , are determined by solving the linear equations

$$\begin{aligned} \sum_{l=1}^n \sum_{j=1}^{N_l-1} Q_l^j & \left[\cos(\theta_l - \theta_m) \log \left| \frac{z_{mk} - \zeta_{lj}}{z_{mk} - \zeta_{lj+1}} \right| - \sin(\theta_l - \theta_m) \arg \frac{z_{mk} - \zeta_{lj}}{z_{mk} - \zeta_{lj+1}} \right] - P_m \\ & = -\text{Im}(e^{-i\theta_m} z_{mk}), \\ z_{mk} & \in C_m, \quad k = 1, \dots, N_m, \quad m = 1, \dots, n. \end{aligned} \quad (28)$$

Using the approximate mapping function, we have the following:

Remark 3 The coefficients of the Laurent expansion (8) is given by

$$a_k \simeq A_k = -\frac{i}{k} \sum_{l=1}^n e^{i\theta_l} \sum_{j=1}^{N_l-1} Q_l^j (\zeta_{lj}^k - \zeta_{lj+1}^k), \quad k = 1, 2, \dots \quad (29)$$

which is equal to (20) because $Q_l^{N_l-1} = -Q_{lN_l}$.

5 Supplementary comments

If we apply the charge simulation method to the unknown function in the form

$$a(z) \simeq A(z) = Q_0 + \sum_{l=1}^n \sum_{j=1}^{N_l} Q_{lj} \log(z - \zeta_{lj}) \quad (30)$$

after the previous approaches, Eq.(7), we have the following formulae corresponding to Scheme 1, Remark 1, Scheme 2 and Remark 2 in the preceding section.

Scheme 4 When each boundary curve C_l is starlike with respect to its inside point ζ_{l0} , a continuous scheme of the approximate mapping function is given by

$$F(z) = z + A(z), \quad A(z) = \sum_{l=1}^n \sum_{j=1}^{N_l} Q_{lj} \log \frac{z - \zeta_{lj}}{z - \zeta_{l0}}, \quad (31)$$

where the unknown constants Q_{lj} , together with P_m , are determined by solving the linear equations

$$\sum_{j=1}^{N_l} Q_{lj} = 0, \quad l = 1, \dots, n, \quad (32)$$

$$\begin{aligned} \sum_{l=1}^n \sum_{j=1}^{N_l} Q_{lj} \left[-\sin \theta_m \log \left| \frac{z_{mk} - \zeta_{lj}}{z_{mk} - \zeta_{l0}} \right| + \cos \theta_m \arg \frac{z_{mk} - \zeta_{lj}}{z_{mk} - \zeta_{l0}} \right] - P_m \\ = -\operatorname{Im} (e^{-i\theta_m} z_{mk}), \\ z_{mk} \in C_m, \quad k = 1, \dots, N_m, \quad m = 1, \dots, n. \end{aligned} \quad (33)$$

Remark 4 The coefficients of the Laurent expansion (8) is given by

$$a_k \simeq A_k = -\frac{1}{k} \sum_{l=1}^n \sum_{j=1}^{N_l} Q_{lj} \zeta_{lj}^k, \quad k = 1, 2, \dots. \quad (34)$$

Scheme 5 The same as Scheme 4 except that (33) changes into

$$\begin{aligned} \sum_{l=1}^n \sum_{j=1}^{N_l} Q_{lj} \left[-\sin \theta \log \left| \frac{z_{mk} - \zeta_{lj}}{z_{mk} - \zeta_{l0}} \right| + \cos \theta \arg \frac{z_{mk} - \zeta_{lj}}{z_{mk} - \zeta_{l0}} \right] - P_m \\ = -\operatorname{Im} (e^{-i\theta} z_{mk}), \\ z_{mk} \in C_m, \quad k = 1, \dots, N_m, \quad m = 1, \dots, n. \end{aligned} \quad (35)$$

Remark 5 The same as Remark 4.

Scheme 4 seems simpler than Scheme 1, and Remark 4 than Remark 1. However, (35) in Scheme 5 is more complex than (23) in Scheme 2. Moreover, the linear equations in Schemes 4 and 5 are ill-conditioned if (i) one of the boundary curves, e.g. C_m , has a symmetry, (ii) $\theta_m = 0$, and (iii) N_m is even.

Example 1 Let D be the exterior of a circle $C : |z - \zeta_0| = \rho$, and place collocation points and charge points by

$$\begin{aligned} z_j &= \zeta_0 + \rho e^{i\omega_j}, \quad \zeta_j = \zeta_0 + r e^{i\omega_j}, \quad 0 < r < \rho, \\ \omega_j &= \frac{2(j-1)}{N} \pi, \quad j = 1, \dots, N. \end{aligned}$$

The linear equations to be solved are written into the matrix form $\mathbf{Ax} = \mathbf{b}$, i.e.,

$$\begin{pmatrix} 0 & 1 & \cdots & 1 \\ -1 & & & \\ \vdots & & a_{kj} & \\ -1 & & & \end{pmatrix} \begin{pmatrix} P \\ Q_1 \\ \vdots \\ Q_N \end{pmatrix} = \begin{pmatrix} 0 \\ -y_1 \\ \vdots \\ -y_N \end{pmatrix}, \quad a_{kj} = \arg \frac{z_k - \zeta_j}{z_k - \zeta_0}, \\ k, j = 1, \dots, N.$$

In this case, it is easy to see that $a_{kj} = 0$ for $j = k$ and $a_{kj} = -a_{jk}$ for $j \neq k$, i.e., the coefficient matrix \mathbf{A} is skew-symmetric. Then $|\mathbf{A}| = {}^t\mathbf{A}| = |-\mathbf{A}| = (-1)^{N+1}|\mathbf{A}|$, and $|\mathbf{A}| = 0$ if N is even.

The ill-conditioning may occur for multiply connected domains, and also for the ellipse, Cassini's oval, etc., as shown later. In practice, we can avoid this difficulty by using an odd N_m . However, Schemes 4 and 5 are not recommendable.

6 Numerical examples

Computations were carried out on a dual Intel Xeon 3.06 GHz processor workstation with the Intel Fortran compiler in double precision working. The IMSL library was used for solving linear equations. Scheme 1 was used unless otherwise specified.

Example 2 The problem domain D is the exterior of three disks,

$$C_l : |z - \zeta_{l0}| = \rho_l, \quad \zeta_{l0} = 3(2 - l), \quad \rho_l = 1, \quad l = 1, 2, 3.$$

Collocation points and charge points are placed by

$$\begin{aligned} z_{lj} &= \zeta_{l0} + \rho_l e^{i\omega_j}, \quad \zeta_{lj} = \zeta_{l0} + q\rho_l e^{i\omega_j}, \quad \omega_j = \frac{2(j-1)}{N}\pi, \\ j &= 1, \dots, N, \quad l = 1, 2, 3, \end{aligned} \quad (36)$$

where $0 < q < 1$ is a parameter for charge placement. Errors are estimated by

$$\epsilon_{F_l} = \max_{1 \leq k' \leq M} |\text{Im}(e^{-i\theta_{l'}} F(z_{lk'})) - P_l|, \quad l = 1, 2, 3, \quad (37)$$

$$\epsilon_{P_l} = P_l - P_l^{(2N)}, \quad l = 1, 2, 3, \quad (38)$$

where $z_{lk'}$ are M ($= 8N$) points uniformly placed on C_l , and $P_l^{(2N)}$ are the results for $2N$ simulation charges.

Figure 2 illustrates by square meshes the numerical conformal mapping of D onto the linear slit domains, (a) $\theta_1 = 0.1\pi$, $\theta_2 = 0.2\pi$, $\theta_3 = 0.3\pi$, (b) $\theta_1 = 0$, $\theta_2 = 0.2\pi$, $\theta_3 = 0.3\pi$ and (c) $\theta_1 = \pi/3$, $\theta_2 = -\pi/3$, $\theta_3 = \pi/3$. Small dots inside the boundary circles are the charge points.

Table 1 shows numerical results of the conformal mapping Fig. 2a, where κ is the L_1 condition number of the coefficient matrix to be solved, and the values of P_l are shown until a nonzero digit appears in the right-hand side of (38). We can see typical features of the charge simulation method as follows. High accuracy is achieved for $F(z)$, and higher for P_l . As a function of N , ϵ_{F_l} and ϵ_{P_l} decay exponentially, however large κ may be. Though not shown in the table, as q decreases from 1 to 0, i.e., the charges move away from the boundary, ϵ_{F_l} and ϵ_{P_l} at first decay exponentially, however large κ may be. The coefficient matrix is singular for $q = 0$.

Table 2 shows numerical results for the coefficients of the Laurent expansion (8) approximated by (20), which gradually diverge to ∞ . The values of A_k are shown until

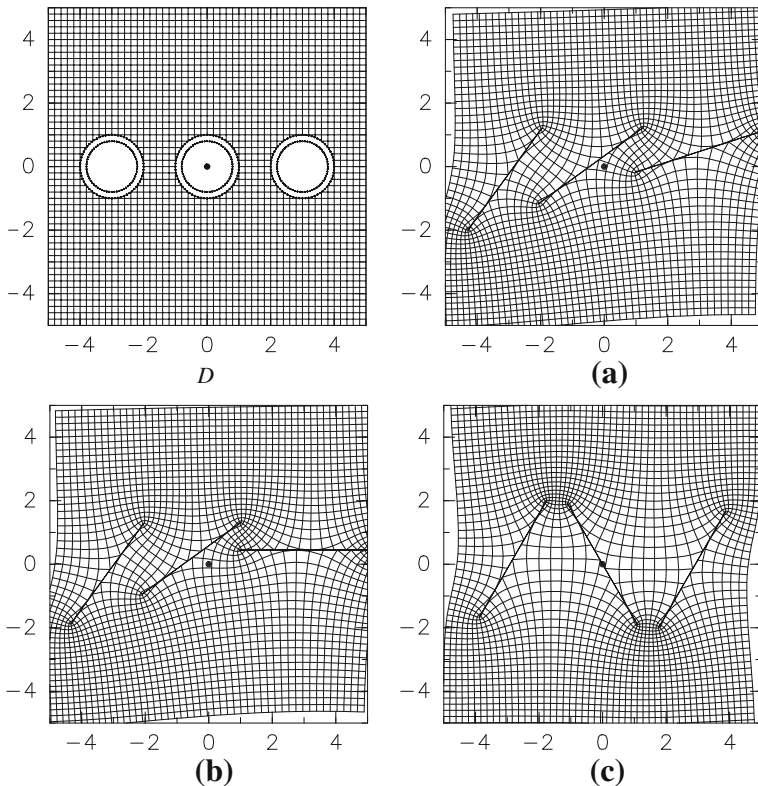


Fig. 2 Numerical conformal mappings of an unbounded triply connected domain D onto the linear slit domains, **a** $\theta_1 = 0.1\pi$, $\theta_2 = 0.2\pi$, $\theta_3 = 0.3\pi$, **b** $\theta_1 = 0$, $\theta_2 = 0.2\pi$, $\theta_3 = 0.3\pi$ and **c** $\theta_1 = \pi/3$, $\theta_2 = -\pi/3$, $\theta_3 = \pi/3$ (Example 2, $N = 64$, $q = 0.8$)

a nonzero digit appears in $A_k - A_k^{(2N)}$, where $A_k^{(2N)}$ are the results for $2N$ simulation charges.

Table 3 shows numerical results of the conformal mapping Fig. 2b by using Scheme 4, where $\theta_1 = 0$. Ill-conditioning occurs for $N = 64$, 66 with an error increase only on C_1 , but not for $N = 63$, 65 as stated in Sect. 5. Scheme 1 is free from this difficulty.

Table 4 shows numerical results of the conformal mapping Fig. 2c, and Table 5 for the coefficients of the Laurent expansion. In this case, $p_1 + p_3 = 0$, $p_2 = 0$ and $a_{2k} = 0$, $k = 1, 2, \dots$ form the symmetry to $z = 0$ and $w = 0$, i.e., $f(-z) = -f(z)$.

Figure 3 illustrates the numerical conformal mapping of D onto the parallel slit domain, (d) $\theta_1 = \theta_2 = \theta_3 = \theta = \pi/3$. It is well-known as a canonical slit domain [34], and is important in the problem of potential flows. This figure illustrates in D streamlines of a uniform flow past three cylindrical obstacles of outlines C_1 , C_2 , C_3 by drawing contour lines of $\text{Im}(e^{-i\theta} F(z))$, where $e^{-i\theta} F(z)$ is the approximated complex velocity potential of the flow [31]. Numerical behavior is similar to Tables 4 and 5, because $p_1 + p_3 = 0$, $p_2 = 0$ and $a_{2k} = 0$, $k = 1, 2, \dots$ form the same symmetry $f(-z) = -f(z)$.

Table 1 Numerical results of the conformal mapping Fig. 2a ($q = 0.8$)

N	ϵ_{F_l}	ϵ_{P_l}	P_l	κ
16				
C_1	9.6E–03	2.2E–03	–0.476	
C_2	9.5E–03	1.1E–03	0.271	4.8E+01
C_3	9.5E–03	1.0E–04	2.2996	
32				
C_1	1.3E–04	3.1E–05	–0.47414	
C_2	1.3E–04	1.5E–05	0.27212	6.0E+02
C_3	1.4E–04	1.4E–05	2.29861	
64				
C_1	5.3E–08	1.2E–08	–0.47410924	
C_2	5.2E–08	5.8E–09	0.272131810	4.2E+04
C_3	5.3E–08	5.5E–09	2.298598835	
128				
C_1	3.1E–14			
C_2	1.4E–13			1.1E+08
C_3	2.0E–13			

Table 2 Numerical results for the Laurent expansion of the mapping Fig. 2a ($N = 64, q = 0.8$)

k	($\text{Re } A_k, \text{ Im } A_k$)	($ A_k , \arg A_k$)
1	(4.41871940E–01, 2.54694233E+00)	(2.58E+00, 1.40)
2	(3.44385978E+00, –6.49029865E–01)	(3.50E+00, –0.19)
3	(3.10290079E+00, 1.40720590E+01)	(1.44E+01, 1.35)
4	(3.08910454E+01, –6.2387936E+00)	(3.15E+01, –0.20)
5	(3.05781267E+01, 1.26224471E+02)	(1.30E+02, 1.33)
6	(2.76735987E+02, –6.1764556E+01)	(2.84E+02, –0.22)
7	(2.92974778E+02, 1.13320923E+03)	(1.17E+03, 1.32)
8	(2.48150956E+03, –5.9718375E+02)	(2.55E+03, –0.24)
9	(2.76397261E+03, 1.01787235E+04)	(1.05E+04, 1.31)
10	(2.22692037E+04, –5.6770108E+03)	(2.30E+04, –0.25)
20	(1.30505451E+09, –3.8612167E+08)	(1.36E+09, –0.29)

Table 3 Numerical results of the conformal mapping Fig. 2b by Scheme 4 ($q = 0.8$)

N	ϵ_{F_1}	ϵ_{F_2}	ϵ_{F_3}	κ
63	3.9E–08	5.4E–08	5.9E–08	2.6E+05
64	5.7E–03	4.2E–08	4.6E–08	5.0E+17
65	2.4E–08	3.3E–08	3.6E–08	3.4E+05
66	5.2E–03	2.6E–08	2.9E–08	9.3E+17

Table 4 Numerical results of the conformal mapping Fig. 2c ($q = 0.8$)

N	ϵ_{F_l}	ϵ_{P_l}	P_l	κ
16				
C_1	1.2E-02	1.2E-04	-2.5275	
C_2	1.2E-02	3.7E-15	4E-16	5.0E+01
C_3	1.2E-02	1.2E-04	2.5275	
32				
C_1	1.6E-04	1.7E-06	-2.527647	
C_2	1.6E-04	5.1E-15	-4E-15	6.0E+02
C_3	1.6E-04	1.7E-06	2.527647	
64				
C_1	6.4E-08	6.7E-10	-2.5276492161	
C_2	6.4E-08	3.3E-15	-1E-15	4.2E+04
C_3	6.4E-08	6.7E-10	2.5276492161	
128				
C_1	4.1E-14			
C_2	1.0E-12			1.1E+08
C_3	6.6E-13			

Table 5 Numerical results for the Laurent expansion of the mapping Fig. 2c ($N = 64, q = 0.8$)

k	($\text{Re } A_k, \text{ Im } A_k$)	($ A_k , \arg A_k$)
1	(-1.25190982E+00, 8.5519740E-01)	(1.52E+00, 2.54)
2	(-3E-14, 4E-14)	(5.62E-14,)
3	(-8.2803292E+00, 1.68461022E+01)	(1.88E+01, 2.02)
4	(-3E-13, 2.50E-13)	(3.81E-13,)
5	(-7.6452477E+01, 1.49351195E+02)	(1.68E+02, 2.04)
6	(-3E-12, 1.8E-12)	(3.31E-12,)
7	(-7.0027999E+02, 1.32678120E+03)	(1.50E+03, 2.06)
8	(-2E-11, 1.6E-11)	(2.75E-11,)
9	(-6.3854447E+03, 1.18175652E+04)	(1.34E+04, 2.07)
10	(-3E-10, 2.7E-10)	(3.85E-10,)
19	(-3.87961349E+08, 6.7896499E+08)	(7.82E+08, 2.09)
20	(-6E-04, 7E-05)	(5.76E-04,)

Figure 4a–c respectively illustrate streamlines of uniform flows past the linear slits of Fig. 2a–c by drawing contour lines of $\text{Im} [e^{-i\theta} F_\theta(F^{-1}(w))]$, where $F_\theta(z)$ is the mapping function of Fig. 3d and $F(z)$ are those of Fig. 2a–c. This method is available for flows in arbitrary direction. However, it is not available for linear slits arbitrarily given because they are determined by D together with the mapping functions.

Example 3 The problem domain D is the exterior of a circle, a Cassini's oval and an ellipse,

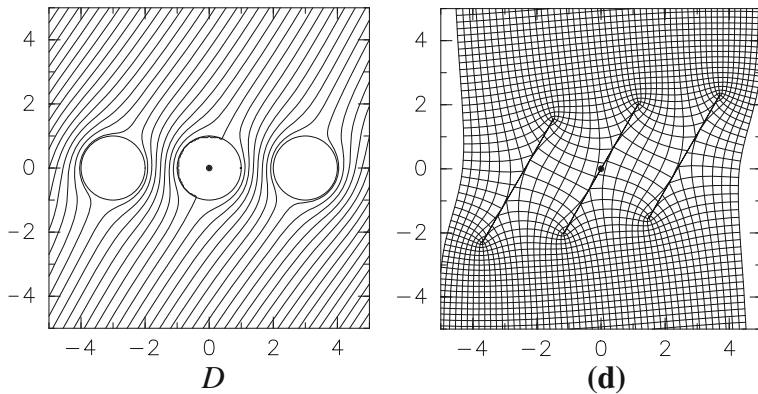


Fig. 3 Numerical conformal mapping of D onto the parallel slit domain, $\mathbf{d} \theta_1 = \theta_2 = \theta_3 = \theta = \pi/3$, where streamlines of a uniform potential flow past three cylindrical obstacles are illustrated in D (Example 2, $N = 64$, $q = 0.8$)

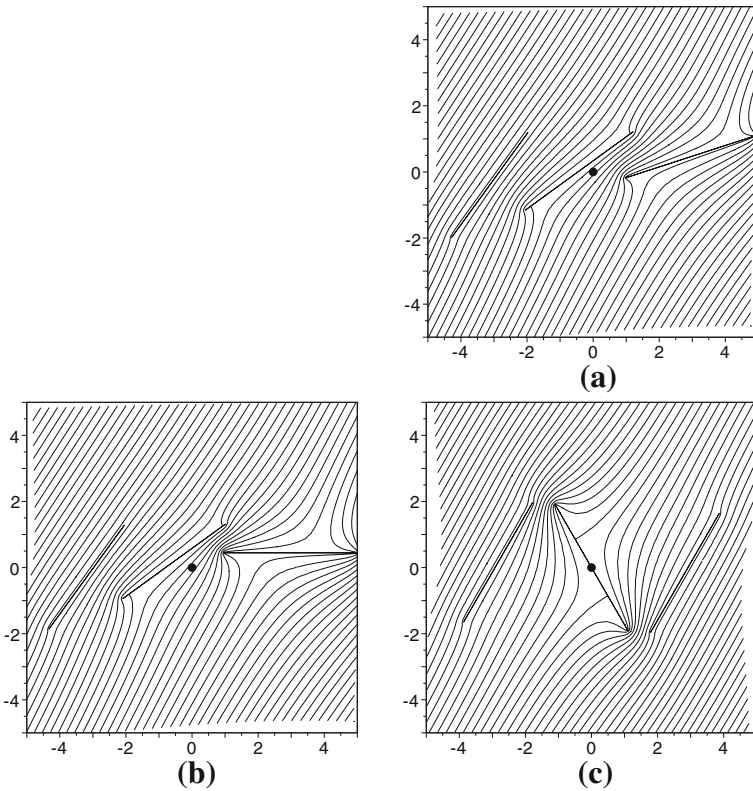


Fig. 4 Streamlines of uniform flows past the linear slits of Fig. 2a–c

$$\begin{aligned} C_1 : |z - \zeta_{10}| &= \rho, \quad \rho = 1, \\ C_2 : |(z - \zeta_{20})^2 - 1| &= \alpha^2, \quad \alpha = 1.06, \end{aligned}$$

$$C_3 : \frac{(x - \operatorname{Re} \zeta_{30})^2}{a^2} + (y - \operatorname{Im} \zeta_{30})^2 = 1, \quad a = 2,$$

$$\zeta_{l0} = 3e^{i\omega_l}, \quad \omega_l = \frac{2(l-1)}{3}\pi, \quad l = 1, 2, 3.$$

For the circle C_1 , collocation points z_{1j} and charge points ζ_{1j} are placed by (36). For Cassini's oval C_2 , collocation points are placed by

$$z_{2j} = \zeta_{20} + \rho_j e^{i\omega_j}, \quad \rho_j = \sqrt{\cos 2\omega_j + \sqrt{\cos^2 2\omega_j + \alpha^4 - 1}},$$

$$\omega_j = \frac{2(j-1)}{N}\pi, \quad j = 1, \dots, N, \quad (39)$$

then charge points by

$$\zeta_{2j} = z_{2j} + iq^*(z_{2j+1} - z_{2j-1}), \quad j = 1, \dots, N, \quad (40)$$

where $q^* > 0$ is another parameter for charge placement, and $z_{20} = z_{2N}$, $z_{2N+1} = z_{21}$. For the ellipse C_3 , in terms of Joukowski's transformation

$$J(t) = \frac{\sqrt{a^2 - 1}}{2} \left(t + \frac{1}{t} \right), \quad (41)$$

collocation points and charge points are placed by

$$z_{3j} = \zeta_{30} + J(\rho e^{i\omega_j}), \quad \zeta_{3j} = \zeta_{30} + J(r e^{i\omega_j}), \quad (42)$$

$$\rho = \sqrt{\frac{a+1}{a-1}}, \quad r = 1 + q(\rho - 1), \quad \omega_j = \frac{2(j-1)}{N}\pi, \quad j = 1, \dots, N,$$

where $0 < q < 1$ is a parameter for charge placement.

Figure 5 illustrates the numerical conformal mapping of D onto the linear slit domain, (a) $\theta_1 = \pi/3$, $\theta_2 = 0$, $\theta_3 = -\pi/3$. Table 6 shows numerical results of the conformal mapping. High accuracy is achieved also for Cassini's oval C_2 and the ellipse C_3 . Table 7 shows numerical results for the coefficients of the Laurent expansion, which spirally diverge to ∞ . It should be noted that Scheme 4 leads to a singular matrix for the parameters in Table 6, where $\theta_2 = 0$ and N are even.

Figure 6 illustrates the numerical conformal mapping of D onto the parallel slit domain, (b) $\theta_1 = \theta_2 = \theta_3 = \theta = \pi/3$, and streamlines of a uniform potential flow past three cylindrical obstacles of outlines C_1 , C_2 , C_3 . Accuracy of the numerical results is almost the same as shown in Tables 6 and 7.

Charge points as well as collocation points play an important role in the charge simulation method. Their optimal location is still an open problem. However, Eq. (40) used for Cassini's oval is available for various shapes of boundary curves consisting of circles and/or ellipses. It is easy to find a nearly optimal value of q^* , since the error at first decreases rapidly as a function of q^* , and then turns to increase.

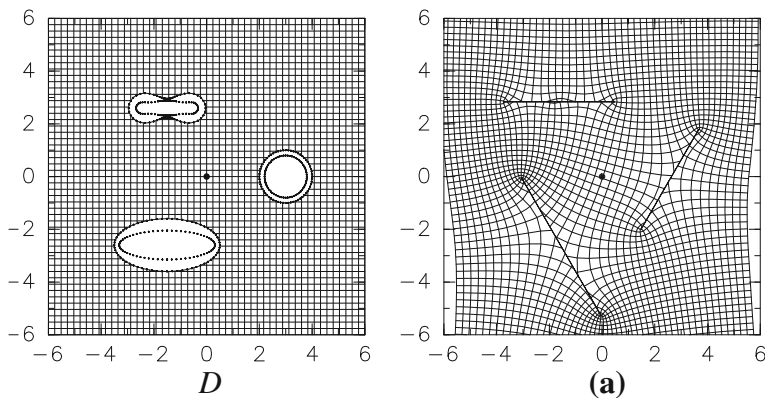


Fig. 5 Numerical conformal mapping of an unbounded triply connected domain D onto the linear slit domain, **a** $\theta_1 = \pi/3$, $\theta_2 = 0$, $\theta_3 = -\pi/3$ (Example 3, $N = 64$)

Table 6 Numerical results of the conformal mapping Fig. 5a

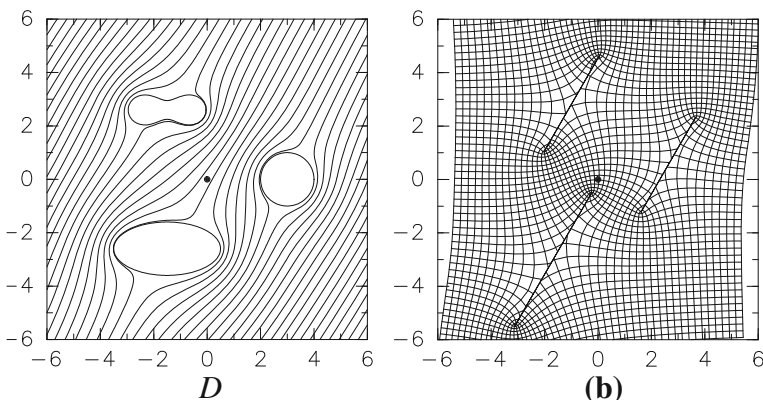
N	q, q^*	ϵ_{F_l}	ϵ_{P_l}	P_l	κ
16					
C_1	0.8	1.0E-02	1.2E-03	-2.278	
C_2	0.25	5.4E-02	3.3E-04	2.8343	7.5E+01
C_3	0.5	1.2E-02	1.3E-03	-2.669	
32					
C_1	0.8	1.4E-04	7.0E-06	-2.278914	
C_2	0.5	5.4E-04	4.5E-07	2.8346624	1.0E+03
C_3	0.5	1.4E-04	5.0E-06	-2.667995	
64					
C_1	0.8	5.5E-08	5.1E-09	-2.278920763	
C_2	1.0	6.5E-07	2.9E-09	2.834662824	1.1E+05
C_3	0.5	3.4E-08	8.1E-09	-2.667990182	
128					
C_1	0.8	4.0E-14			
C_2	2.0	1.3E-11			3.2E+09
C_3	0.5	6.3E-13			

7 Concluding remarks

We have proposed a numerical method for the conformal mapping of unbounded multiply connected domains onto the linear slit domain, where the angles of slits to the real axis are arbitrarily assigned. It gives approximate mapping functions of simple form with high accuracy, and the coefficients of the Laurent expansion that appears in the mapping theorem as well. The charge simulation method is suited for domains of smooth boundaries, especially for circular domains. Therefore the methods proposed

Table 7 Numerical results for the Laurent expansion of the mapping Fig. 5a ($N = 64$)

k	$(\operatorname{Re} A_k, \operatorname{Im} A_k)$	$(A_k , \arg A_k)$
1	$(-1.78385359E+00, -9.38347574E-01)$	$(2.01E+00, -2.66)$
2	$(-5.22201078E+00, 1.184829549E+01)$	$(1.29E+01, 1.99)$
3	$(1.51210975E+01, -3.8856506E+00)$	$(1.56E+01, -0.25)$
4	$(-5.6105401E+01, -4.8024772E+00)$	$(5.63E+01, -3.06)$
5	$(-4.12662203E+01, 2.73598802E+02)$	$(2.77E+02, 1.72)$
6	$(1.6287880E+02, -4.0780095E+02)$	$(4.39E+02, -1.19)$
7	$(-1.92779718E+03, 1.93698045E+03)$	$(2.73E+03, 2.35)$
8	$(3.782630269E+03, 2.4025703E+03)$	$(4.48E+03, 0.57)$
9	$(-1.24468404E+04, -1.33680380E+04)$	$(1.83E+04, -2.32)$
10	$(-2.1298974E+04, 1.20757976E+05)$	$(1.23E+05, 1.75)$
20	$(-1.72295320E+10, 4.20976514E+10)$	$(4.55E+10, 1.96)$

**Fig. 6** Numerical conformal mapping of D onto the parallel slit domain, **b** $\theta_1 = \theta_2 = \theta_3 = \theta = \pi/3$, where streamlines of a uniform potential flow past three cylindrical obstacles are illustrated in D (Example 3, $N = 64$)

here and in [3, 4, 6, 41] are suited for mapping the canonical circular domains onto the canonical slit domains. However, the solvability of the linear equations is still an open problem, together with the convergence of the solution. Some of computations and drawings of figures are implemented as a toolbox of numerical conformal mappings for Scilab of INRIA. Although the toolbox is not yet ready for public use, we would like to open it for public in the future.

The charge simulation method, or the fundamental solution method, in a more general context has been applied also to the conformal mapping of periodic structure domains [35] and Stokes flows past obstacles in a periodic array [37–40], where various types of periodic fundamental solutions are used.

In addition, it is recently clarified that an effective biological flight is realized due to interactions between vortices and solid-body boundaries. For instance, a certain kind of plant seeds are falling with rotation very slowly and stably by trapping a vortex

created from its leading edge [30], and butterflies gain effective lift by generating a sequence of vortices by flapping their wings [24]. In a theoretical study of these flight mechanism, it is considered that, regarding slits as solid bodies, the relation between their arrangement and vortices should be elucidated. On the other hand, the dynamics of point vortices in the presence of many obstacles is now developed. Sakajo [42] gave the equation of motion for N point vortices in the canonical circular domain, and discussed the case of general multiply connected domains assuming the conformal mapping function onto the circular domain. The combination of this equation of motion and the numerical conformal mapping proposed here might help elucidating the relation between slit arrangement and vortices.

Numerical conformal mappings onto the spiral slit domain [34] and in particular onto the circular domain [21] are interesting problems left for future studies.

Acknowledgments The authors wish to thank Emeritus Prof. M. Shiba (Hiroshima University) and Prof. T. Sakajo (Hokkaido University) for their helpful discussion.

Open Access This article is distributed under the terms of the Creative Commons Attribution License which permits any use, distribution, and reproduction in any medium, provided the original author(s) and the source are credited.

References

1. Amano, K.: Numerical conformal mapping based on the charge simulation method (in Japanese). *Trans. Inform. Process. Soc. Japan* **28**, 697–704 (1987)
2. Amano, K.: A charge simulation method for the numerical conformal mapping of interior, exterior and doubly-connected domains. *J. Comput. Appl. Math.* **53**, 353–370 (1994)
3. Amano, K.: A charge simulation method for numerical conformal mapping onto circular and radial slit domains. *SIAM J. Sci. Comput.* **19**, 1169–1187 (1998)
4. Amano, K., Okano, D., Ogata, H., Shimohira, H., Sugihara, M.: A systematic scheme of numerical conformal mappings of unbounded multiply-connected domains by the charge simulation method (in Japanese). *IPSJ J.* **42**, 385–395 (2001)
5. Amano, K., Ootori, H., Li, T., Endo, K., Okano, D.: Numerical conformal mappings onto a rectilinear slit domain by the charge simulation method (in Japanese). *IPSJ J.* **50**, 1775–1779 (2009)
6. Amano, K., Okano, D.: A circular and radial slit mapping of unbounded multiply connected domains. *JSIAM Lett.* **2**, 53–56 (2010)
7. Benchama, N., DeLillo, T.K., Hrycak, T., Wang, L.: A simplified Fornberg-like method for the conformal mapping of multiply connected regions—comparisons and crowding. *J. Comput. Appl. Math.* **209**, 1–21 (2007)
8. Crowdy, D.G.: Analytical solutions for uniform potential flow past multiple cylinders. *Eur. J. Mech. B Fluids* **25**, 459–470 (2006)
9. Crowdy, D.G., Marshall, J.: Conformal mappings between canonical multiply connected domains. *Comput. Methods Funct. Theory* **6**, 59–76 (2006)
10. DeLillo, T.K., Horn, M.A., Pfaltzgraff, J.A.: Numerical conformal mapping of multiply connected regions by Fornberg-like methods. *Numer. Math.* **83**, 205–230 (1999)
11. DeLillo, T.K., Elcrat, A.R., Pfaltzgraff, J.A.: Schwarz–Christoffel mapping of multiply connected domains. *J. Anal. Math.* **94**, 17–47 (2004)
12. DeLillo, T.K., Driscoll, T.A., Elcrat, A.R., Pfaltzgraff, J.A.: Radial and circular slit maps of unbounded multiply connected circle domains. *Proc. R. Soc. Lond. Ser. A Math. Phys. Eng. Sci.* **464**, 1719–1737 (2008)
13. Driscoll, T.A., Trefethen, L.N.: Schwarz–Christoffel Mapping. Cambridge University Press, Cambridge (2002)
14. Fornberg, B.: A numerical method for conformal mappings. *SIAM J. Sci. Stat. Comput.* **1**, 386–400 (1980)

15. Fornberg, B.: A numerical method for conformal mapping of doubly connected regions. *SIAM J. Sci. Stat. Comput.* **5**, 771–783 (1984)
16. Gaier, D.: *Konstruktive Methoden der konformen Abbildung*. Springer, Berlin (1964)
17. Gaier, D.: Integralgleichungen erster Art und konforme Abbildung. *Math. Z.* **147**, 113–129 (1976)
18. Gaier, D.: Das logarithmische Potential und die konforme Abbildung mehrfach zusammenhängender Gebiete. In: Butzer, P.L., Fehér, F. (eds.) E.B. Christoffel, The Influence of his Work on Mathematics and the Physical Sciences, pp. 290–303. Birkhäuser, Basel (1981)
19. Gutknecht, M.H.: Numerical conformal mapping methods based on function conjugation. *J. Comput. Appl. Math.* **14**, 31–77 (1986)
20. Hayes, J.K., Kahaner, D.K., Kellner, R.G.: An improved method for numerical conformal mapping. *Math. Comput.* **26**, 327–334 (1972)
21. Henrici, P.: *Applied and Computational Complex Analysis*, vol. 3. Wiley, New York (1986)
22. Hough, D.M., Papamichael, N.: The use of splines and singular functions in an integral equation method for conformal mapping. *Numer. Math.* **37**, 133–147 (1981)
23. Hough, D.M., Papamichael, N.: An integral equation method for the numerical conformal mapping of interior, exterior and doubly-connected domains. *Numer. Math.* **41**, 287–307 (1983)
24. Iima, M., Yanagita, T.: Is a two-dimensional butterfly able to fly by symmetric flapping? *J. Phys. Soc. Japan* **70**, 5–8 (2001)
25. Katsurada, M., Okamoto, H.: A mathematical study of the charge simulation method I. *J. Fac. Sci. Univ. Tokyo Sect. IA Math.* **35**, 507–518 (1988)
26. Katsurada, M., Okamoto, H.: The collocation points of the fundamental solution method for the potential problem. *Comput. Math. Appl.* **31**, 123–137 (1996)
27. Kitagawa, T.: On the numerical stability of the method of fundamental solution applied to the Dirichlet problem. *Japan J. Appl. Math.* **5**, 123–133 (1988)
28. Koebe, P.: Abhandlungen zur Theorie der konformen Abbildung IV, Abbildung mehrfach zusammenhängender schlichter Bereiche auf Schlitzbereiche. *Acta Math.* **41**, 305–344 (1916)
29. Kythe, P.K.: *Computational Conformal Mapping*. Birkhäuser, Boston (1998)
30. Lentink, D., Dickinson, W.B., Leeuwen, J.L. van , Dickinson, M.H.: Leading-edge vortices elevate lift of autorotating plant seeds. *Science* **324**, 1438–1440 (2009)
31. Milne-Thomson, L.M.: *Theoretical Hydrodynamics*. Dover, New York (1996)
32. Murashima, S., Kuhara, H.: An approximate method to solve two-dimensional Laplace's equation by means of superposition of Green's functions on a Riemann surface. *J. Inform. Process.* **3**, 127–139 (1980)
33. Murota, K.: Comparison of conventional and “invariant” schemes of fundamental solutions method for annular domains. *Japan J. Indust. Appl. Math.* **12**, 61–85 (1995)
34. Nehari, Z.: *Conformal Mapping*. McGraw-Hill, New York (1952)
35. Ogata, H., Okano, D., Amano, K.: Numerical conformal mapping of periodic structure domains. *Japan J. Indust. Appl. Math.* **19**, 257–275 (2002)
36. Ogata, H., Okano, D., Sugihara, M., Amano, K.: Unique solvability of the linear system appearing in the invariant scheme of the charge simulation method. *Japan J. Indust. Appl. Math.* **20**, 17–35 (2003)
37. Ogata, H., Amano, K., Sugihara, M., Okano, D.: A fundamental solution method for viscous flow problems with obstacles in a periodic array. *J. Comput. Appl. Math.* **152**, 411–425 (2003)
38. Ogata, H.: A fundamental solution method for three-dimensional Stokes flow problems with obstacles in a planar periodic array. *J. Comput. Appl. Math.* **189**, 622–634 (2006)
39. Ogata, H., Amano, K.: A fundamental solution method for three-dimensional viscous flow problems with obstacles in a periodic array. *J. Comput. Appl. Math.* **193**, 302–318 (2006)
40. Ogata, H., Amano, K.: A fundamental solution method for two-dimensional Stokes flow problems with one-dimensional periodicity. *Japan J. Indust. Appl. Math.* **27**, 191–215 (2010)
41. Okano, D., Ogata, H., Amano, K., Sugihara, M.: Numerical conformal mappings of bounded multiply connected domains by the charge simulation method. *J. Comput. Appl. Math.* **159**, 109–117 (2003)
42. Sakajo, T.: Equation of motion for point vortices in multiply connected circular domains. *Proc. R. Soc. Lond. Ser. A Math. Phy. Eng. Sci.* **465**, 2589–2611 (2009)
43. Shiba, M.: On the Riemann–Roch theorem on open Riemann surfaces. *J. Math. Kyoto Univ.* **11**, 495–525 (1971)
44. Singer, H., Steinbigler, H., Weiss, P.: A charge simulation method for the calculations of high voltage fields. *IEEE Trans. Power Apparatus. Syst.* **PAS-93**, 1660–1668 (1974)
45. Symm, G.T.: An integral equation method in conformal mapping. *Numer. Math.* **9**, 250–258 (1966)

-
- 46. Symm, G.T.: Numerical mapping of exterior domains. *Numer. Math.* **10**, 437–445 (1967)
 - 47. Symm, G.T.: Conformal mapping of doubly-connected domains. *Numer. Math.* **13**, 448–457 (1969)
 - 48. Trefethen, L.N. (ed.) *Numerical Conformal Mapping*. North-Holland, Amsterdam (1986)